A&A 436, 661–669 (2005)
DOI: 10.1051/0004-6361:20040511

Astronomy & Astrophysics

VLT/UVES spectroscopy of the O supergiant companion to 4U 1907+09(7)⋆

N. L. J. Cox[1], L. Kaper[1], and M. R. Mokiem[1]

Astronomical Institute "Anton Pannekoek", University of Amsterdam, Kruislaan 403, 1098 SJ Amsterdam, The Netherlands
e-mail: ncox@science.uva.nl

Received 24 March 2004 / Accepted 2 March 2005

Abstract. High-resolution optical spectra of the high-mass X-ray binary 4U 1907+09 covering the wavelength range 4680–10 400 Å indicate that the X-ray pulsar's massive companion is an O8/O9 supergiant with a dense stellar wind. The interstellar atomic lines of Na I and K I of this strongly reddened source ($E_{(B-V)}$ = 3.45 mag) are used to set a lower limit to its distance: $d \approx 5$ kpc, excluding the possibility that the massive companion is a Be star. We re-evaluate the system parameters; the new spectral classification of 4U 1907+09's O supergiant companion is discussed in the context of its similarity in X-ray and orbital properties to Wray 15-977/GX 301-2. The Hα line shows variability similar to what is observed in other wind-fed systems. A remarkable feature is the strong He II 4686 Å emission line, which possibly originates in the accretion flow towards the X-ray pulsar.

Key words. stars: binaries: close – stars: early-type – stars: winds, outflows – X-rays: individual: 4U 1907+09 – ISM: lines and bands

1. Introduction

The optical counterpart to the X-ray pulsar 4U 1907+09 (also referred to as 4U 1907+097) (Giacconi et al. 1971) is a heavily reddened massive star (V = 16.4 mag) showing broad Hα emission (Schwartz et al. 1980), identifying the system as a high-mass X-ray binary (HMXB). The X-ray flux is produced by the accretion of material from the massive companion's stellar wind onto the neutron star. HMXBs are divided into two subclasses: the majority (~80%) of systems host a Be star, a rapidly rotating B main-sequence star or (sub)giant with a dense equatorial disk producing strong and variable Hα emission. The corresponding X-ray sources are often transients showing a strong increase in X-ray emission when the compact object in its eccentric orbit passes through the Be-star disk. The second class comprises the OB-supergiant systems where the compact object orbits through a dense stellar wind (see Kaper 2001 for a review). As soon as the supergiant exceeds its Roche lobe, the mass-transfer rate increases significantly, resulting in a much higher X-ray luminosity (~10^{38} instead of 10^{35-36} erg s^{-1}) and, if the compact object is a pulsar, a much shorter spin period (seconds rather than minutes).

X-ray pulsations with a period of 437.5 s were discovered in 4U 1907+09 with the *Tenma* satellite (Makishima et al. 1984). Subsequent pulse-timing analyses with EXOSAT (Cook & Page 1987) and, more recently, with the *Rossi X-ray Timing Explorer* (RXTE) (In 't Zand et al. 1998) have resulted in the accurate determination of the X-ray pulsar's orbital parameters: orbital period $P_{\rm orb}$ = 8.3753 d, and eccentricity e = 0.28. In the orbital period vs. pulse period diagram (Corbet 1986; Waters & Van Kerkwijk 1989) 4U 1907+09 is located in the region occupied by the wind-fed OB supergiant systems; Be/X-ray binaries tend to have much longer orbital periods (30–200 d) than those with supergiants (1–10 d).

Whether the massive companion to 4U 1907+09 is an OB supergiant or a Be star is still a matter of debate. The main reason for this is that the strong reddening and faintness of the source hamper the detection of its optical spectrum. Schwartz et al. (1980) suggested that the massive star is an OB supergiant. On the other hand, Iye (1986) proposed that it is a Be star. Besides the spectral properties of the star, the latter author considered the periodic flaring in the X-ray light curve of the system similar to what is observed in Be/X-ray binaries. A severe problem with the Be-star classification is the strong interstellar absorption spectrum towards the source, which is not consistent with the relative proximity of the system (≲1 kpc) when it is a Be star and not a luminous OB supergiant. Extended optical spectroscopy of the system by Van Kerkwijk et al. (1989) resulted in an almost certain classification of the massive companion as a B supergiant.

In recent studies of the X-ray properties of 4U 1907+09, however, the Be-star nature of the optical companion has been reconsidered, mainly in order to explain the periodic flaring of the X-ray source just before periastron passage

⋆ Based on observations made at the European Southern Observatory, Paranal, Chile (ESO program 67.C-0281).

(In 't Zand et al. 1998; Roberts et al. 2001; Mukerjee et al. 2001). In this respect it is interesting to mention Wray 15-977, the massive companion to the X-ray pulsar GX 301-2, which is classified as a B1.5 Ia+ hypergiant (Kaper et al. 1995; Koh et al. 1997) and exhibits an X-ray flare close to periastron passage similar to 4U 1907+09. Obviously, a definite spectral classification of the massive companion to 4U 1907+09 is required to better understand the physical conditions in the system and its similarity to Wray 15-977/GX 301-2.

Another reason to study the optical spectrum of 4U 1907+09 is its very rich interstellar spectrum. It can be used to set a lower limit to the distance of the source based on the radial velocity interval covered by the interstellar absorption lines and a model describing the differential rotation of the Milky Way. Also, this heavily reddened object ($E_{(B-V)}$ = 3.45 mag, Sect. 5.1) provides a nice opportunity to investigate the properties of the diffuse interstellar bands (DIBs) at unprecedented strength. This line of investigation is discussed in a companion paper (Cox et al. 2005).

In this paper we present high-resolution optical spectra of the massive companion to 4U 1907+09 obtained with the Ultraviolet and Visual Echelle Spectrograph (UVES) mounted at the *Very Large Telescope* (VLT) of the European Southern Observatory in Paranal, Chile. The dataset and the applied reduction procedures are described in the next section. The spectrum is used to perform a new spectral classification of the massive star based on a comparison with state of the art model spectra (Sect. 3), to set a lower limit to the distance of the system and to re-evaluate the binary system parameters (Sects. 4 and 5).

Table 1. Properties of the observed target 4U 1907+09 and the telluric standards HD 165470 and HD 166934. The listed values were obtained from the SIMBAD database, except $E_{(B-V)}$, $v_r \sin i$ and spectral type of the optical companion to 4U 1907+09 which are taken from this study. The intrinsic colours for the quoted spectral types are adopted from Schmidt-Kaler (1982). The ephemeris used to calculate the orbital phase is taken from In 't Zand et al. (1998): P_{orb} = 8.3753(1) d; $T_{peri} = T_{-30°}$ = MJD 50 132.00 (6). The instrument settings are indicated by the selected central wavelength (in Å) of the red and blue arm of the UVES spectrograph, respectively.

	4U 1907+09	HD 165470	HD 166934
RA (J2000)	19 09 37.9	18 07 54.37	18 13 40.8
Dec (J2000)	+09 49 49	–38 33 55.5	–18 49 30
l (deg)	43.74	353.92	11.96
b (deg)	0.48	–8.79	–0.51
V (mag)	16.37	7.34	8.8
$B-V$	3.17	–0.17	–0.2
Spectral type	O8-O9 I	B2 III	B2 IV/V
$(B-V)_0$	–0.27	–0.24	–0.24
$E_{(B-V)}$ (mag)	3.45	0.07	0.04
$v_r \sin i$ (km s^{-1})	100 ± 5	43 ± 3	54 ± 4
Exposure time (s)	see below	200	760
UT at start (2001-09-23)	see below	23:30:40	23:47:54
Airmass (sec z)	1.3–1.8	1.055	1.055

		4U 1907+09			
UT at start (2001)	MJD	Orbital phase	UVES setting	t_{exp} (s)	airmass
mm-dd-time	(–2 400 000)				
09-24/01:02:02	52 176.04422	244.06	437+860	2700	1.30–1.45
09-26/01:48:35	52 178.07656	244.30	346+580	2700	1.49–1.79
09-27/00:57:36	52 179.04117	244.42	346+580	1800	1.32–1.42
09-27/01:28:32	52 179.06263	244.43	346+580	1800	1.42–1.57

2. Observations and data reduction

High-resolution ($R \sim 40\,000$) spectra of the optical companion to the X-ray pulsar 4U 1907+09 were obtained with the UVES (Kaufer et al. 2000) on the VLT during the nights of 24 to 27 September, 2001. Observations were performed under excellent conditions at Paranal, with a relative humidity of less than 10% and seeing between 0.4 and 0.8 arcsec. The total exposure time was 9000 s, for four exposures on 4U 1907+09, and 760 and 200 s on each of the telluric standard stars, respectively. Table 1 lists some observational details, as well as some properties of the optical companion to 4U 1907+09. Two telluric standard spectra were taken at about similar airmass, although not during the same night, nor at the same position on the sky, to perform the correction for telluric absorption lines in the red part of the spectrum.

The spectra were reduced using the UVES context within the MIDAS reduction package (version 02SEPpl1.2), which allows to apply the UVES data reduction pipeline software and to adapt the standard procedures where required. The raw echelle frames were first bias corrected; then the individual echelle orders were traced using the Hough algorithm. Flatfield correction was done by extracting the flatfield and subsequent (order by order) division of the science frame by the flatfield. The orders were extracted with an optimal extraction routine and merged applying a running mean (the individual orders can be accessed for cross-check purposes). The resulting signal-to-noise ratio (*S/N*) ranges from 5 (green) to about 100 in the red continuum. Wavelength calibration is based on ThAr arc spectra. For a calibration exposure over 1200 arc lines are identified and fitted for each of the CCDs and set-ups. The typical root mean square for these fits is about 0.003 Å in the blue and 0.008 Å in the red, i.e., better than one fifth of a pixel. We found no significant quality differences compared to the products delivered by the pipeline. However, one should be cautious with any features near the echelle order overlaps, since artifacts are prone to emerge. Especially, for wavelengths longwards of 8000 Å we had to inspect the individual orders for spurious features, and since the quality of the first 5 to 10 Å of the order is poor, we clipped the edges.

Telluric lines mainly pose a problem in the wavelength region longwards of 6800 Å. This part of the spectrum, with the exception of regions free of telluric lines, was corrected for telluric absorption lines. Note that the photospheric lines present in the telluric standard star spectrum (of spectral type B) need to be removed before applying the telluric correction. As two telluric standards are available one can check for possible artifacts resulting from the division.

The original spectrum is divided by the telluric standard raised to the power α, where we take the ratio of the airmass of both observations as the initial guess. To improve the spectrum further it may be necessary to shift the telluric standard spectrum by small amount, typically one or a fraction of a wavelength bin. The optimum values for both the airmass correction

factor α and the wavelength shift (in fractions of bins) were obtained using an iterative procedure that minimizes the residual noise.

3. The photospheric spectrum of 4U 1907+09 's massive companion

The photospheric properties of early-type stars are best studied in the ultraviolet wavelength domain where their spectral energy distribution peaks, or in the blue part of the optical spectrum where traditionally the OB-star spectral classification is performed. However, due to the strong reddening towards 4U 1907+09, these spectral domains are severely attenuated and practically inaccessible with state of the art instrumentation. With VLT/UVES it now has become feasible to study the green ($\gtrsim$4600 Å) and red spectrum of 4U 1907+09 at sufficient spectral resolution to determine the photospheric and wind properties of the faint early-type companion.

We show a selection of the observed stellar lines (Fig. 1) that are most relevant for assigning a spectral type. The spectrum is shown in its entirety, for its rich complex of interstellar features, in Cox et al. (2005). Due to the high reddening of the line of sight towards 4U 1907+09 the signal-to-noise is very poor in the green part of the spectrum, although it is still sufficient to show the presence of the He I 4713 Å and Hβ (4861 Å) lines. Moving towards the near-infrared the signal-to-noise improves as the effect of interstellar extinction strongly reduces, and the spectrum reveals a wealth of stellar and interstellar features.

In the following subsections we describe the photospheric spectrum of the OB-type companion to 4U 1907+09. A comparison to model spectra results in the determination of the stellar parameters.

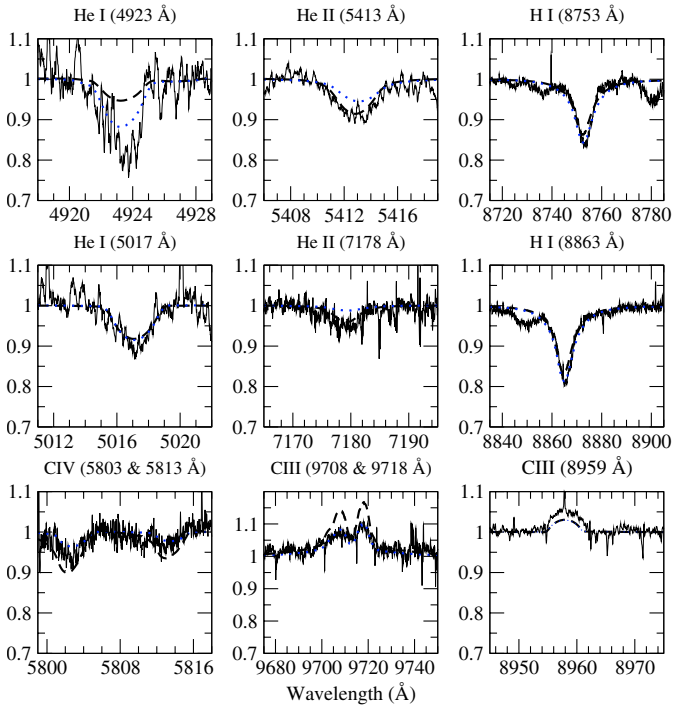

Fig. 1. A representative sample of photospheric lines (solid) is shown with two model spectra (O9 I = dotted and O8 I = dashed.). The parameters adopted for both stellar models are listed in Table 2. The O8 I model represents the observed spectrum very well, except for the He I line at 4923 Å. Adopting a later type (i.e. O9 I) increases the He I absorption. Obviously, this decreases the strength of the He II lines at 5413 and 7178 Å. On the other hand, the O9 I model fits the C IV and C III lines best.

3.1. Description of the spectrum

The spectrum of the massive companion to 4U 1907+09 is dominated by lines of hydrogen and helium, characteristic of early-type spectra. The presence of He II lines in the spectrum indicates that the spectral type is O rather than B. Several HMXBs with OB-supergiant primary have He II 4686 Å in emission (e.g. Cyg X-1, Gies & Bolton 1986), but this line is more likely formed in the accretion flow rather than in the stellar photosphere. Together with the detection of He II 5411.5 Å (Fig. 1) and 10 123.6 Å (Fig. 1 in Cox et al. 2005) absorption lines, this clearly points to an O-type spectrum. Further strong evidence in favour of an O7 to O9 type supergiant is the C IV absorption at 5803 Å and 5813 Å (Fig. 1). However, in order to further constrain the spectral type we compare the observed spectrum with a grid of modelled atmospheric spectra in the next section. In the stellar spectrum Hα shows strong emission and the Hβ and He I 5876 Å lines have a P Cygni type profile indicating a dense stellar wind. Figure 2 shows three wind lines (He II at 4685.7 Å, He I at 5875.7 Å, and Hα at 6562.8 Å) on a velocity scale at three different orbital phases: (1) $\phi = 0.30$, (2) $\phi = 0.42$ and (3) $\phi = 0.43$. The He I 5876 Å line remains almost constant while the Hα line exhibits clear variability in its line center. Such variations are commonly observed in wind-fed systems similar to 4U 1907+09 (e.g. Vela X-1) and are likely due to a photo-ionization wake trailing the X-ray source in its orbit (Blondin et al. 1990; Kaper et al. 1994).

The most remarkable feature in the spectrum of 4U 1907+09 is the strong emission reaching nearly three times the continuum level at the position of the He II 4686 Å line (Fig. 2). At the red side of the line two other emission lines are present, like the He II line varying in strength; equivalent widths for the feature at 4697.2 Å are 0.9 ± 0.1, 0.4 ± 0.2 and 0.7 ± 0.2 Å for the three orbital phases (0.30, 0.42 and 0.43), respectively. For the other unidentified line at 4705.6 Å the corresponding equivalent width values are 0.5 ± 0.2, 0.2 ± 0.1 and 0.5 ± 0.1 Å. Although these emission lines could be redshifted He II lines (at ~725 and ~1275 km s^{-1}), their physical nature is unclear. A possibility may be that these emission lines are Raman scattered EUV emission lines originating near the He II Ly γ transition at 243 Å. He II ions in the stellar wind scatter these EUV photons in the wing of the upper energy level of the He II Pf α transition at 4686 Å, such that the EUV photons are transformed into blue photons near the downward transition of He II 4686 Å. Raman scattering has been observed in another O supergiant system (HD 153919/4U 1700-37), but here the emission lines are found near the He II 1640 Å (Baα) transition in the UV domain (Kaper et al. 1990).

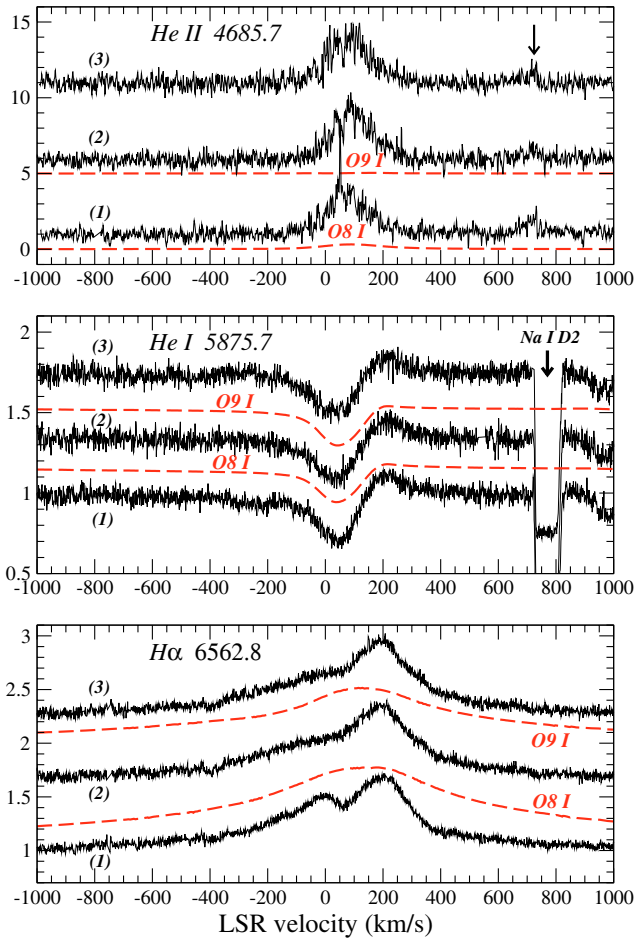

Fig. 2. Normalised spectra, on a local standard of rest (LSR) velocity scale, of three spectral lines formed in the stellar wind of the companion to the X-ray pulsar 4U 1907+09 observed at the three different orbital phases (Sect. 3.1): Hα (*bottom*), He I at 5876 Å (*middle*) and He II at 4686 Å (*top*). Two model spectra of type O8 I and O9 I (grey-dashed) are shown on the same scale. All spectra are normalized to unity, but plotted with a vertical offset for clarity. It is clear that the standard model does not reproduce the wind lines as well as it fits the photospheric lines. The arrow in the top panel indicates one of the two unidentified emission features discussed in the text (Sect. 3.1).

3.2. Comparison with model spectra

To further constrain the stellar parameters of the optical companion of 4U 1907+09 we used a grid of model spectra to compare to the observed green and red part of the spectrum. The spectral type is then derived by calculating the *EW* ratio of the He I 4471 Å and the He II 4542 Å lines (Mathys 1988) extracted from the model that describes the red part of the spectrum best.

A grid of non-LTE unified photosphere/wind models (Lenorzer et al. 2004) is used, calculated with the CMFGEN code of Hillier & Miller (1998). CMFGEN solves the equations of radiative transfer in an atmosphere with an outflowing stellar wind subject to the constraints of radiative and statistical equilibrium, while still using a complexity of input physics and atomic models similar to the work of Lanz & Hubeny (2003). For a full description of the applied techniques and physical details of the model we refer to Hillier & Miller (1998). The grid is calculated by one of us (MRM) and has been employed for studies of optical and near-IR spectral features of O-type stars (Lenorzer et al. 2004; Puls et al. 2005). It consists of unified stellar atmosphere/wind models for early-type main sequence stars, giants and supergiants, for which the basic stellar parameters ($T_{\rm eff}$, $M_\star$ and $R_\star$) are taken from the calibration of Vacca et al. (1996). In these models the hydrostatic photosphere is smoothly connected to the stellar wind. For the velocity structure of the wind a typical beta velocity law with $\beta = 1.0$ is adopted (see Lenorzer et al. 2004). The adopted mass-loss rate is based on the predictions by Vink et al. (2000, 2001). The wind terminal velocity v_∞ (which is usually derived from UV resonance lines) was taken from the scaling relation with the escape velocity $v_{\rm esc}$ (Lamers et al. 1995). For our comparison the Lanz & Hubeny O-star grid is not adequate since it gives only spectral coverage until 7500 Å, and thus does not include the Paschen series. The latter is used by us to constrain $\log g$. More importantly, the Lanz & Hubeny hydrostatic/plane parallel model can not take effects of mass-loss into account. Therefore, it does not allow for a direct comparison of the wind lines, nor for treating the filling in of photospheric lines by wind emission (e.g. Fig. 5 in Mokiem et al. 2004).

In Fig. 1 (photospheric lines) we show the two models from the model grid which, based on the hydrogen and helium lines, reproduce the observed lines best. To facilitate a comparison with the observed line profiles, the synthetic line profiles were convolved with a rotational broadening profile. Given the parameter sampling of the model grid, the parameter which is best constrained from these two models is the effective temperature $T_{\rm eff}$. For the spectral range investigated here this sampling is ~1500 K. The relative strengths of the He I and He II lines react strongly on this parameter and we find that models with $T_{\rm eff}$ lower than ~29 500 K or higher than ~31 500 K show large discrepancies in these lines compared to observations. Given this range in $T_{\rm eff}$ we find that the gravity sensitive hydrogen line wings are best fitted with a low value for $\log g \sim 3$. This parameter is not as well constrained as $T_{\rm eff}$, due to the course grid sampling in $\log g$. However, from our comparison we find that this value is a good estimate for the surface gravity of the star.

In Table 2 we list the parameters of the two models for which we find the best correspondence with the observed spectrum. Note that these models have been calculated adopting solar abundances. As high-mass X-ray binaries have undergone a phase of mass transfer, one might expect that the chemical surface abundance of the mass gainer, i.e. the current O supergiant, is enhanced with nuclearly processed material. In this context, Blaauw (1993) suggested that OB runaways produced through the binary supernova channel (these systems followed a similar evolutionary path as HMXBs) have a higher helium surface abundance and higher rotation rate than ordinary OB stars. However, a recent analysis by Repolust et al. (2004) demonstrates that the helium abundance of O stars shows a large spread (helium abundance ϵ ranges from 0.08 to 0.20, with an average of 0.10), and the O runaways do not show a higher helium abundance than the other O stars in their sample. Given the correspondence between the models and observations of 4U 1907+09, we find no indications that its helium surface abundance is significantly different from other O stars.

Table 2. Parameters of the two stellar models from the stellar atmosphere grid that match the observed spectrum best.

Stellar Parameter	Model #1 O8 Ia	Model #2 O9 Ia
$T_{\rm eff}$	31 240 K	29 760 K
$\log g$	3.074	3.017
$M_\star$	27.9 $M_\odot$	26.0 $M_\odot$
$L_\star$	5.5×10^5 $L_\odot$	4.8×10^5 $L_\odot$
$v_{\rm r} \sin i$	100 km s^{-1}	100 km s^{-1}
$R_\star$	25.4 $R_\odot$	26.2 $R_\odot$
$\dot{M}$	9.2×10^{-6} $M_\odot$ yr^{-1}	6.0×10^{-6} $M_\odot$ yr^{-1}
v_∞	1730 km s^{-1}	1690 km s^{-1}

The adopted $v_{\rm r} \sin i$ is 100 km s^{-1} and was estimated from the observed width of the He I lines. This value is in accordance with the determination by Iye (1986) and by Van Kerkwijk et al. (1989) who found values of 92 ± 15 km s^{-1} and 80 ± 9 km s^{-1}, respectively, from He I 5876 Å line measurements. However, the spectra used by these authors were of insufficient spectral resolution to resolve the P Cygni shape of this line, which is affected by the strong stellar mass loss. As a consequence, their adopted FWHM value is too small. When using the observed width of e.g. the photospheric He I 10315 Å line, we obtain $v \sin i = 100 \pm 5$ km s^{-1}, taking into account the width of the UVES instrumental profile ($FWHM_{\rm inst} = 0.15$–0.20 Å).

The photospheric lines are best matched with O8 (model #1) to O9 (model #2) supergiant spectra. The wind lines (e.g. Hα, He I 5876 Å) in these model spectra are, however, to weak compared to the observations. In order to obtain a better correspondence, models with a mass-loss rate enhanced by a factor 2, 2.5 and 3 were calculated. Such an increase is still in the range spanned by the difference between mass-loss determinations (e.g. Puls et al. 1996) and mass-loss predictions (e.g. Vink et al. 2000). With a 2.5 times higher mass-loss rate the model fits the wind lines much better (Fig. 2). The observed He II 4686 Å line is still much stronger than the models predict; however, as we indicated before it is likely that the formation mechanism of this line is different.

We note that a better agreement between the predicted and observed strength of the wind lines can also be achieved by modifying the velocity law. Namely, a higher value for β results in a more slowly accelerating wind and through the continuity equation in a higher density in the line forming region of Hα and He I 5876 Å. In the case of a density sensitive line like Hα, which strength scales with the density squared, one would expect an increase in emission for higher values of β. In Fig. 2 we also see that the shape of the observed Hα emission is not optimally reproduced by the model, indicating that a larger value of β would be more appropriate. For a more accurate determination of the mass-loss rate the velocity field of the stellar outflow must be known more precisely. However, the required ultraviolet part of the spectrum containing strong resonance lines formed in the stellar wind (e.g. Groenewegen & Lamers 1989) is not accessible. We conclude that the mass-loss rate of the optical companion to 4U 1907+09 is not too high for a luminous (Ia) late-O supergiant.

Both Be (main-sequence or subgiant) stars and OB supergiants have Hα in emission. A main-sequence star model does, however, not provide a good fit to the observed spectrum: the line profiles are too narrow (i.e. $\log g$ must be small) and the wind lines indicate a much higher (factor ~100) mass-loss rate than common in main-sequence stars. Also, the FWHM of the Hα emission is about 1200 km s^{-1}, much larger than typically observed in Be stars (Dachs 1987). Therefore, the Hα profile also supports our interpretation that the companion to 4U 1907+09 is a supergiant rather than a Be star. In the next section we will provide additional arguments supporting this conclusion.

4. Distance to the HMXB system 4U 1907+09

In this section we discuss methods to determine the distance to the binary system 4U 1907+09. We use the velocity profile of the interstellar atomic lines together with the galactic velocity gradient that links radial velocity to distance, and thus provides a lower limit to the distance of 4U 1907+09. Furthermore, we use an extinction map and 2MASS IR photometry to derive the extinction $A_{\rm V}$, and subsequently $R_{\rm V}$ in the direction of 4U 1907+09.

4.1. Distance to 4U 1907+09 from interstellar absorption of Na I and K I

Of the different interstellar atomic species showing transitions in the optical spectrum (Na I, Ca I, Ca II and Ca I) only K I and Na I were detectable, since the signal in the blue part of the spectrum (below 4500 Å) is too low to detect any features. The K I line (at 7700 Å) is shown in Fig. 3, the Na I D2 line (at 5889.95 Å) can be seen in the middle panel of Fig. 2. Both Na I D lines are heavily saturated. The saturated doublet lines D1 and D2 have a lower limit on the equivalent width of 1.69 Å and 1.72 Å, respectively. Nevertheless, these lines can still be used to derive a rough indication of the distance to the system. Using d(pc) = 30.75 EW (Beals & Oke 1953), with EW the equivalent width (in km s^{-1}) of the Na I D line (>85 km s^{-1}), we obtain a conservative value for the distance to the system, $d \sim 2.6$ kpc. Van Kerkwijk et al. (1989) derive from the Na I D lines, using the same relationship, a lower limit of 2.1 ± 0.6 kpc, which agrees well. However, from the radial velocity gradient in this direction (Fig. 3) and the width of the (saturated) Na I line (=70 km s^{-1}) we derive a significantly larger distance, $d \gtrsim 5$–6 kpc.

For the total equivalent width of the K I line we obtain 0.836 ± 0.05 Å; fortunately, one of the two doublet components is not affected by telluric lines. We have fitted the K I profile with a set of six Gaussians, which represents the profile, except the substructure, fairly well.

The K I absorption line clearly shows the different velocity components in the line-of-sight towards 4U 1907+09. We show the galactic velocity gradient as a function of distance towards 4U 1907+09 in the bottom panel of Fig. 3. The 57.6 km s^{-1} velocity component in the K I profile corresponds to a distance of ~4 or ~8 kpc. Components with velocity ≤60 km s^{-1} could, in principle, also be situated beyond 8 kpc. We consider this to

Article published by EDP Sciences and available at http://www.edpsciences.org/aa or http://dx.doi.org/10.1051/0004-6361:20040511

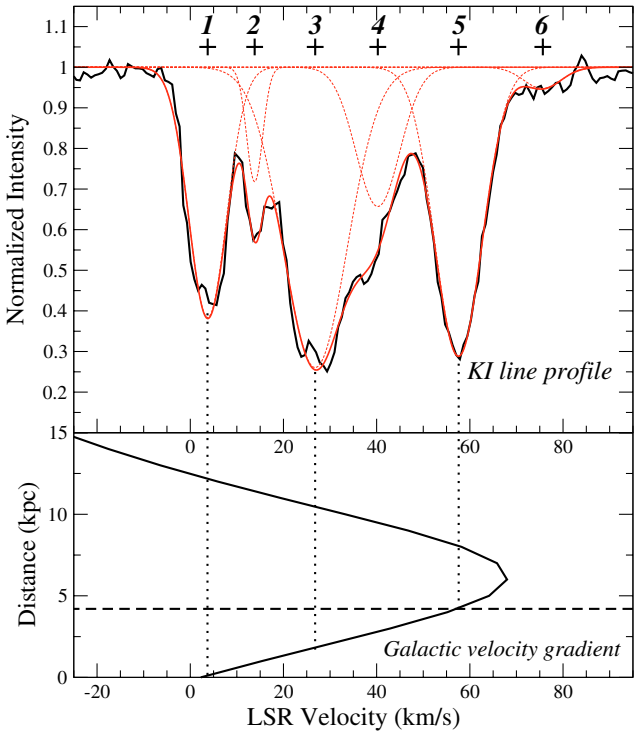

Fig. 3. The K I line clearly shows the complicated velocity structure in this line of sight. The different components are fitted with six Gaussians. The main velocity components of K I are at v = 3.7, 26.8 and 57.6 km s^{-1}.

be unlikely, and we take component 5 to set the lower limit of $d \geq 4$ kpc. A very weak component at 76 km s^{-1} is seen, but it is inconsistent with the computed rotational velocity curve, i.e. the maximum velocity given by the latter is ≈70 km s^{-1}. The accuracy of this simple model hinges on the adopted distance, d = 8.5 kpc, to the galactic center (Eisenhauer et al. 2003, and references therein) and the assumption of circular orbits (Brand & Blitz 1993).

By studying the distribution of H II regions Russeil (2003) constructed a revised model of the Galaxy indicating the location of the different spiral arms. The line of sight toward 4U 1907+09 grazes the Sagittarius-Carina arm over a distance of several kiloparsecs, explaining the extended (velocity) structure of the interstellar medium.

4.2. Extinction and distance from extinction maps

From the spatial distribution of the interstellar extinction we have an additional diagnostic to estimate the distance to 4U 1907+09. Cahn (1973) shows that at about 2 to 4 kpc the line of sight crosses the Sagittarius Arm. From Fig. 9 a in Neckel et al. (1980) it appears that the line of sight suffers from a relatively modest amount of visual extinction per unit distance (A_V/kpc < 1.0 mag kpc^{-1}) for distances larger than 1 kpc. The total extinction up to 3 kpc is $A_V \leq 5$ mag. Note that only in few directions (e.g. Cyg OB2) an extinction of 10 mag (up to $d \leq 3$ kpc) has been measured.

Recently, Drimmel et al. (2003) constructed a 3D extinction model for the Galaxy based on COBE data. Galactic extinction can be estimated for any distance in any direction. From their maps we retrieve for the direction of 4U 1907+09 at a distance of 4 kpc an A_V of 6.86 mag which would be consistent with the measured $E_{(B-V)}$ (Sect. 5.1) if R_V = 2.0. For the calculation of the total extinction we adopted a rescaling of the disk, rather than of the spiral structure, which is in better agreement with observations in this direction (see also the top right panel in Fig. 10 in Drimmel et al. 2003). This result implies an uncomfortably low value of R_V. For a distance of 5 kpc the extinction map yields an A_V of 9.3 mag, implying that R_V = 2.7. Apparently, the extinction increases strongly as a function of distance for this line of sight.

We note here that adopting the observed 2MASS (Cutri et al. 2003) infrared colours *JHK* (9.995, 9.242 & 8.774 mag) together with intrinsic colours for O8/9 Ia type supergiants from Wegner (1994) results, via the equations in Fitzpatrick (1999), in $R_V = 2.75 \pm 0.12$, and subsequently A_V = 9.5 mag. The error includes uncertainties in the intrinsic colours of supergiant OB stars and in the empirical relationship between colour excess and R_V. Clearly, this is in agreement with the visual extinction derived from the galactic extinction map. The three methods evaluated above indicate that the distance to the system is ∼5 kpc.

5. Evaluation of system parameters

In the following we investigate whether the stellar parameters derived from the model comparison are consistent with other observational constraints on the system, like the reddening, distance, X-ray luminosity, and Roche-lobe radius of the primary. We adopt $T_{\rm eff}$ = 30 500 K and $\log g$ = 3.1 based on the model spectra (spectral type O8-O9 Ia, cf. Table 2).

5.1. Luminosity, mass-loss rate, radius and spectroscopic mass of the O supergiant

The models used to fit the spectrum yield a luminosity of 4.8–5.5 × 10^5 $L_\odot$ and a radius of 25.4–26.2 $R_\odot$ (Table 2). The intrinsic colour of an O8-O9 Ia star is $(B-V)_0 = -0.27$ mag (Schmidt-Kaler 1982); with the observed $(B-V) = 3.17 \pm 0.06$ mag (Schwartz et al. 1980) this results in a colour excess $E_{(B-V)}$ = 3.45 mag. The severe reddening towards 4U 1907+09 makes the spectroscopic distance c.q. luminosity determination very sensitive to the precise value of R_V. Together with R_V = 2.7, the distance d = 5 kpc and $V = 16.37 \pm 0.02$ mag, this gives an absolute visual magnitude of the O supergiant $M_V = -6.3 \pm 0.2$ mag. Given the bolometric correction BC = -3.05 ± 0.14 mag (Schmidt-Kaler 1982), the luminosity of the O8-O9 supergiant becomes $L = 4.3 \pm 0.7 \times 10^5$ $L_\odot$, i.e. similar to the luminosity corresponding to the model atmosphere.

Therefore, in the following we adopt a luminosity of 5 × 10^5 $L_\odot$. With $\log g$ = 3.1 and R = 26 $R_\odot$ one obtains a "spectroscopic" mass for the O supergiant of 27 $M_\odot$. The "evolutionary" mass seems to be higher based on the position of the companion of 4U 1907+09 in the Hertzsprung-Russell diagram (Fig. 4), on the order of 40 $M_\odot$ assuming that the massive companion to 4U 1907+09 is evolving to the red. If it were to come back to the blue, the evolutionary mass is more consistent with

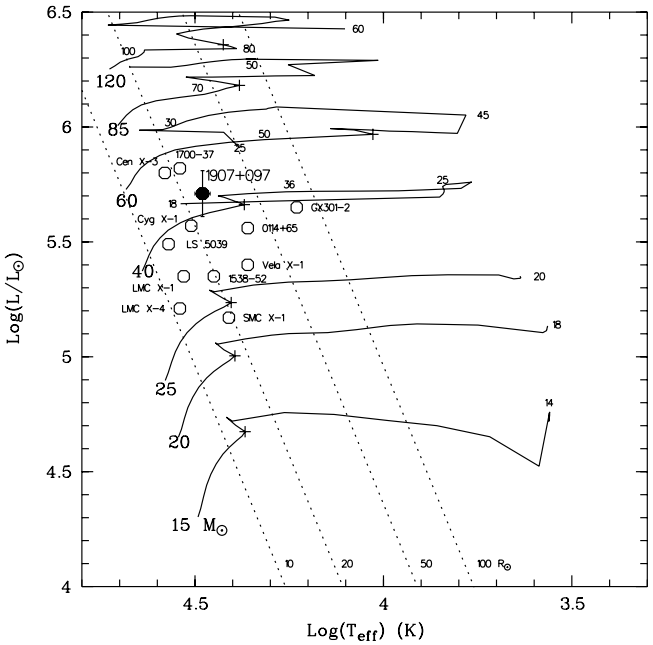

Fig. 4. The position of 4U 1907+09 (filled circle) in the Hertzsprung-Russell diagram compared to other OB supergiant systems (open circles). The evolutionary tracks (from single stars) are from Lejeune & Schaerer (2001); the initial mass is indicated. The + symbol refers to the point of core-hydrogen exhaustion. Due to mass loss the stellar mass decreases along the tracks (as shown by the smaller font numbers). Assuming that 4U 1907+09 is evolving to the red, its current evolutionary mass would be of the order of 40 $M_\odot$.

the spectroscopic mass, i.e. it would have decreased to about 25 $M_\odot$. The model radius of 26 $R_\odot$ is in accordance with the current position in the HRD.

If 4U 1907+09 is on its way to become a red supergiant and its mass is 27 $M_\odot$, the current position in the HRD indicates that 4U 1907+09 is overluminous for its mass. Similar behaviour has been observed for other HMXBs with an OB supergiant companion (Conti 1978; Kaper 2001). This may be due to the evolutionary history of the system including a phase of mass transfer from the neutron star progenitor to the now O8-O9 supergiant. In some systems evidence is also found for nuclear enrichment of the OB companion, but in 4U 1907+09 we encounter normal elemental abundances (Sect. 3.2).

5.2. X-ray luminosity, Roche-lobe radius, and radial-velocity orbit

According to In 't Zand et al. (1997) the mean X-ray luminosity of 4U 1907+09 is $L_X = 8 \times 10^{34} d_{\rm kpc}^2$ erg s^{-1}. At a distance of 5 kpc L_X becomes $2.0{\times}10^{36}$ erg s^{-1}; such a luminosity is typical for wind-fed systems (e.g. Kaper 1998). The X-ray lightcurve shows a strong peak at periastron passage (Marshall & Ricketts 1980). The predicted Bondi-Hoyle X-ray accretion luminosity, adopting the parameters derived above (and a terminal wind velocity of 1750 km s^{-1} for a late O supergiant), is of the same order of magnitude ($\sim 10^{37}$ erg s^{-1} at periastron passage, $\sim 5 \times 10^{35}$ erg s^{-1} at apastron).

In a binary system with zero eccentricity and synchronous rotation, the radius of the primary cannot exceed the Roche-lobe radius:

$$R_L = \frac{0.49a}{0.6 + q^{3/2} \ln(1 + q^{-1/3})}$$

with a the orbital separation between primary and secondary and $q = M_X/M_O$ the ratio in mass of secondary (compact X-ray source) and primary (O supergiant). Adopting $M_X = 1.4\ M_\odot$ (canonical neutron star mass) and $M_O = 27\ M_\odot$, the orbital separation follows from Kepler's third law and the orbital period ($P = 8.3753(1)$ d, In 't Zand et al. 1998); then $a = 54\ R_\odot$, and $R_L = 43\ R_\odot$, i.e. larger than the adopted stellar radius. In eclipsing HMXBs the radius of the primary can be derived from the eclipse duration; it turns out that in those (five) systems the primary radius is about equal to the Roche-lobe radius (Kaper 2001). In 4U 1907+09 we have to adopt a primary mass of about 12 $M_\odot$ to have the primary fitting within its Roche-lobe. However, 4U 1907+09 is an eccentric system ($e = 0.28(4)$, In 't Zand et al. 1998) so that the "Roche-lobe radius" of the primary at periastron passage is $R_L = 31\ R_\odot$, which is close to the adopted stellar radius of 26 $R_\odot$.

The few spectra we obtained do not provide sufficient coverage of the orbit to derive the radial-velocity amplitude K_O of the primary (and, combined with the accurate orbit of the X-ray pulsar a direct constraint on the mass of both components). Van Kerkwijk et al. (1989) give it a try with their dataset using the radial velocity of He I 5876 Å at orbital phase 0.61 and 0.06 (i.e. close to the descending and ascending nodes) and derive a radial-velocity amplitude of 0 ± 16 km s^{-1}. Our VLT/UVES spectra show that this He I line has a P Cygni type profile, disqualifying the line as a proper diagnostic of the radial-velocity orbit of the primary. The photospheric radial velocities we derive (in the heliocentric frame) are: 7 ± 6 km s^{-1} at $\phi_{\rm peri} = 0.06$ (He I 7281 Å and higher H I Paschen lines); 35 ± 8 km s^{-1} at $\phi_{\rm peri} = 0.30$ (He I 4922 and 5016 Å, He II 5412 Å); 59 km s^{-1} at $\phi_{\rm peri} = 0.42$ (only He I 4922 Å, other lines are too weak). Note that in the latter two spectra the (blue-shifted) absorption profile of the He I 5876 Å line is at 13 and 5 km s^{-1}, respectively. For $M_X = 1.4\ M_\odot$, $M_O = 27\ M_\odot$ (adopted) and $K_X = 229$ km s^{-1} (observed) one predicts that $K_O = 12$ km s^{-1}. Our limited data indicate that the radial-velocity amplitude is larger than zero, but for a proper determination more spectra and better orbital coverage is needed.

5.3. Similarity to Wray 15-977 (GX 301-2)

At a distance of 5 kpc the observed parameters of 4U 1907+09 are in excellent agreement with the O8-O9 supergiant model parameters, the predicted X-ray accretion luminosity, and binarity constraints. An overview of the adopted and derived parameters is given in Table 3.

Based on the similarity of their X-ray lightcurves, 4U 1907+09 and GX 301-2 have been compared in recent literature. Both sources show a strong peak in X-ray flux close to periastron passage and (perhaps) a secondary peak near apastron. Also, both systems have a considerable eccentricity

Table 3. Overview of the adopted system parameters of 4U 1907+09. The bottom part of the table lists the parameters of the X-ray source.

Parameter	Value
$T_{\rm eff}$	30 500 K
$\log g$	3.1
$R_\star$	26 $R_\odot$
$M_{\rm O}$ (spectroscopic)	27 $M_\odot$
$M_{\rm O}$ (HRD)	~40 $M_\odot$
$L_{\rm O}$	5×10^5 $L_\odot$
$v_{\rm r} \sin i$	100 km s^{-1}
$\dot{M}$	7×10^{-6} $M_\odot$ yr^{-1}
d	5 kpc
$P_{\rm orb}$	8.3753 d
$P_{\rm spin}$	440.341 s
e	0.28
$T_{\pi/2}$	MJD 50 134.76
ω	330°
$a_{\rm X} \sin i$	83 light seconds
$L_{\rm X}$	2.0×10^{36} erg s^{-1}

($e = 0.28$ and $e = 0.47$, for 4U 1907+09 and GX 301-2, respectively). In 't Zand et al. (1998) suggest that the wind of the supergiants in these systems is not isotropic, but enhanced in the equatorial plane, as suggested in other hot and bright supergiants (e.g. Zickgraf et al. 1996; Ignace et al. 1996). The two X-ray flares in the orbit may then be caused by the neutron star traversing this plane twice per orbit in a sufficiently inclined orbit. Although Roberts et al. (2001) favour a Be-star companion, which is excluded by our observations, they come to a similar conclusion. The trailing stream they propose to account for the observed changes in the absorption column towards the X-ray source may be responsible for the variations we encounter in the Hα profile. The optical spectrum of 4U 1907+09's massive companion is not as extreme as that of Wray 15-977, the B1 Ia+ hypergiant companion to GX 301-2 (Kaper et al. 1995). Wray 15-977 has many more P Cygni-like features in its spectrum, while in 4U 1907+09 only the strongest hydrogen and helium lines have a P Cygni shape. Still, the estimated luminosity and mass-loss rate of the O8-O9 supergiant companion to 4U 1907+09 are high and both systems are positioned on similar evolutionary tracks.

From an evolutionary point of view Wray 15-977/ GX 301-2 is an important system as it sets a lower limit to the initial mass for black-hole formation in a binary (Van den Heuvel & Habets 1984; Kaper et al. 1995; Ergma & Van den Heuvel 1998; Wellstein & Langer 1999). The neutron star was produced by the supernova explosion of the initially most massive star in the system. Depending on whether the mass transfer in the system was conservative or not, the initial mass of the neutron-star progenitor is, respectively, of the same order as the current mass of the secondary (i.e. Wray 15-977) or lower (about 25 $M_\odot$ according to Wellstein & Langer 1999). Apparently the initial mass of the primary was not sufficient to produce a black hole. The evolutionary scenario applied to Wray 15-977/ GX 301-2 by Wellstein & Langer (1999) results in a relatively long orbital period of the system, as is observed ($P_{\rm orb} = 41.5$ d). A shorter orbital period, like in 4U 1907+09, is difficult to accommodate in such a scenario.

Acknowledgements. The authors thank ESO and the Paranal staff for their support in using the UVES instrument on the VLT. Thanks are extended to Arjen van der Meer for his assistance in preparing and executing the observations, and to Pascale Ehrenfreund for valuable discussions. Relevant and clear comments from the referee are greatly appreciated and have helped to improve the paper significantly. We acknowledge support from NOVA and NWO. This research has made use of the SIMBAD database, operated at CDS, Strasbourg, France, and of NASA's Astrophysics Data System. This publication makes use of data products from the Two Micron All Sky Survey, which is a joint project of the University of Massachusetts and the Infrared Processing and Analysis Center/California Institute of Technology, funded by the National Aeronautics and Space Administration and the National Science Foundation. This research made use of the online VizieR database of astronomical catalogues (Ochsenbein et al. 2000).

References

Beals, C. S., & Oke, J. B. 1953, MNRAS, 113, 530
Blaauw, A. 1993, Astron. Soc. Pac. Conf. Ser., 35, 207
Blondin, J. M., Kallman, T. R., Fryxell, B. A., & Taam, R. E. 1990, ApJ, 356, 591
Brand, J., & Blitz, L. 1993, A&A, 275, 67
Cahn, J. H. 1973, A&A, 25, 477
Conti, P. S. 1978, A&A, 63, 225
Cook, M. C., & Page, C. G. 1987, MNRAS, 225, 381
Corbet, R. H. D. 1986, MNRAS, 220, 1047
Cox, N. L. J., Kaper, L., Foing, B. H., & Ehrenfreund, P. 2005, A&A, in press
Cutri, R. M., Skrutskie, M. F., Van Dyk, S., et al. 2003, VizieR Online Data Catalog, 2246, 0
Dachs, J. 1987, in Physics of Be Stars, IAU Coll., 92, 149
Drimmel, R., Cabrera-Lavers, A., & López-Corredoira, M. 2003, A&A, 409, 205
Eisenhauer, F., Schödel, R., Genzel, R., et al. 2003, ApJ, 597, L121
Ergma, E., & Van den Heuvel, E. P. J. 1998, A&A, 331, L29
Fitzpatrick, E. L. 1999, PASP, 111, 63
Giacconi, R., Kellogg, E., Gorenstein, P., Gursky, H., & Tananbaum, H. 1971, ApJ, 165, L27
Gies, D. R., & Bolton, C. T. 1986, ApJ, 304, 389
Groenewegen, M. A. T., & Lamers, H. J. G. L. M. 1989, A&AS, 79, 359
Hillier, D. J., & Miller, D. L. 1998, ApJ, 496, 407
Ignace, R., Cassinelli, J. P., & Bjorkman, J. E. 1996, ApJ, 459, 671
In 't Zand, J. J. M., Baykal, A., & Strohmayer, T. E. 1998, ApJ, 496, 386
In 't Zand, J. J. M., Strohmayer, T. E., & Baykal, A. 1997, ApJ, 479, L47
Iye, M. 1986, PASJ, 38, 463
Kaper, L. 1998, in Properties of Hot Luminous Stars, ASP Conf. Ser., 131, 427
Kaper, L. 2001, in The Influence of Binaries on Stellar Population Studies, ASSL, 264, 125
Kaper, L., Hammerschlag-Hensberge, G., & Takens, R. J. 1990, Nature, 347, 652
Kaper, L., Hammerschlag-Hensberge, G., & Zuiderwijk, E. J. 1994, A&A, 289, 846

Kaper, L., Lamers, H. J. G. L. M., Ruymaekers, E., Van den Heuvel, E. P. J., & Zuiderwijk, E. J. 1995, A&A, 300, 446
Kaufer, A., D'Odorico, S., & Kaper, L. 2000, UVES User Manual
Koh, D. T., Bildsten, L., Chakrabarty, D., et al. 1997, ApJ, 479, 933
Lamers, H. J. G. L. M., Snow, T. P., & Lindholm, D. M. 1995, ApJ, 455, 269
Lanz, T., & Hubeny, I. 2003, ApJS, 146, 417
Lejeune, T., & Schaerer, D. 2001, A&A, 366, 538
Lenorzer, A., Mokiem, M. R., de Koter, A., & Puls, J. 2004, A&A, 422, 275
Makishima, K., Kawai, N., Koyama, K., et al. 1984, PASJ, 36, 679
Marshall, N., & Ricketts, M. J. 1980, MNRAS, 193, 7P
Mathys, G. 1988, A&AS, 76, 427
Mokiem, M. R., Martín-Hernández, N. L., Lenorzer, A., de Koter, A., & Tielens, A. G. G. M. 2004, A&A, 419, 319
Mukerjee, K., Agrawal, P. C., Paul, B., et al. 2001, ApJ, 548, 368
Neckel, T., Klare, G., & Sarcander, M. 1980, A&AS, 42, 251
Ochsenbein, F., Bauer, P., & Marcout, J. 2000, A&AS, 143, 23
Puls, J., Kudritzki, R.-P., Herrero, A., et al. 1996, A&A, 305, 171
Puls, J., Urbaneja, M. A., Venero, R., et al. 2005, A&A, in press
Repolust, T., Puls, J., & Herrero, A. 2004, A&A, 415, 349
Roberts, M. S. E., Michelson, P. F., Leahy, D. A., et al. 2001, ApJ, 555, 967
Russeil, D. 2003, A&A, 397, 133
Schmidt-Kaler, T. 1982, Bulletin d'Information du Centre de Données Stellaires, 23, 2
Schwartz, D. A., Griffiths, R. E., Bowyer, S., Thorstensen, J. R., & Charles, P. A. 1980, AJ, 85, 549
Vacca, W. D., Garmany, C. D., & Shull, J. M. 1996, ApJ, 460, 914
Van den Heuvel, E. P. J., & Habets, G. M. H. J. 1984, Nature, 309, 598
Van Kerkwijk, M. H., Van Oijen, J. G. J., & Van den Heuvel, E. P. J. 1989, A&A, 209, 173
Vink, J. S., de Koter, A., & Lamers, H. J. G. L. M. 2000, A&A, 362, 295
Vink, J. S., de Koter, A., & Lamers, H. J. G. L. M. 2001, A&A, 369, 574
Waters, L. B. F. M., & Van Kerkwijk, M. H. 1989, A&A, 223, 196
Wegner, W. 1994, MNRAS, 270, 229
Wellstein, S., & Langer, N. 1999, A&A, 350, 148
Zickgraf, F.-J., Humphreys, R. M., Lamers, H. J. G. L. M., et al. 1996, A&A, 315, 510